Improving the Efficiency of the NEB Reaction Path Finding Algorithm

IGNACIO FDEZ. GALVÁN, MARTIN J. FIELD
IBS, Institut de Biologie Structurale—Jean-Pierre Ebel, 41 rue Jules Horowitz, F-38027 Grenoble, France, CEA, CNRS, Université Joseph Fourier

Received 17 March 2007; Revised 5 April 2007; Accepted 25 April 2007
DOI 10.1002/jcc.20780
Published online 1 June 2007 in Wiley InterScience (www.interscience.wiley.com).

Abstract: The nudged elastic band (NEB) method is a successful optimization method for obtaining minimum energy reaction paths if only the initial and final structures are known. However, the original implementation of the method had some limitations, which has meant that there has been considerable interest in proposing alternative NEB formulations, which show improved convergence behavior. In this work, we present two modifications to the standard NEB procedure. The first involves the use of a second-order quasi-Newton optimization technique applied separately to each of the images that form the path. The second consists of the use of an interpolating spline to represent the path. This ensures that the images along the path are evenly spaced and means that the arbitrary spring forces employed in the standard NEB method are no longer necessary. We tested these modifications on a set of small, but relatively complex, chemical systems and found that the computation time was reduced by as much as 90% compared with the standard method.

 J Comput Chem 29: 139–143, 2008

Key words: MEP; reaction path; NEB

Introduction

One of the most important problems in current computational chemistry is the identification of the minimum energy path (MEP) for a given process. The MEP is often a good description of the optimum mechanism by which a stable conformation of atoms is converted into another one. The structure with maximum energy along the MEP approximates the transition state for the process and the energy profile itself permits estimation of the transition rates.

For the determination of reaction paths or saddle points a variety of methods have been proposed,[1] ranging from methods that somehow follow the shape of the potential energy surface, either from minima to saddle points or *vice versa*,[2–4] to those that represent the whole path through a set of images (or replicas or states) and try to optimize them in a concerted fashion.[5–8] An efficient and successful method of this last type is the one known as the Nudged Elastic Band (NEB) algorithm, developed by Jónsson et al.[9] Like others in its category, the method starts by defining a number of images of the system between the initial and final states. If the system has N free particles, each image behaves as a point in a $3N$-dimensional space. Spring interactions are then added between adjacent images to form an "elastic band". The optimization of the band, which converges to the MEP, involves a minimization of the forces acting on each image due to both the springs and the system's potential energy. One of the advantages of the NEB method, and others like it, is that knowledge of the location and structure of the saddle point are not needed beforehand.

An essential feature of the NEB method, and one of the reasons for its success, is that the spring forces are projected onto the tangents to the path at each image whereas the image forces arising from the potential energy function are projected onto the hyperplanes that are perpendicular to the path. Although this projection improves the behavior of the NEB algorithm when compared with similar methods, it has the drawback that it makes it difficult to define a target function that defines the path and that can be optimized with second-order methods.

In this work, we present two improvements to the NEB procedure that increase its performance and reduce the computational time needed to locate paths. The first modification involves using a second-order L-BFGS method for the optimization of the individual images along the path whereas the second concerns the replacement of the spring forces between images with a spline description of the path. This allows the redistribution of images at any point in the optimization process without the introduction of external forces.

The rest of the paper is organized as follows. "The NEB Method" section presents a quick overview of the NEB method, "Modifications to the Method" section discusses two possible improvements and proposes a modified method, "Tests and Results"

Correspondence to: I. Fdez. Galván; e-mail: Ignacio.Fernandez-Galvan@ibs.fr

Contract/grant sponsor: Secretaría de Estado de Universidades e Investigación of the Spanish Ministerio de Educación y Ciencia

section details the test cases employed to evaluate the performance of the modifications and the results obtained, and the last section concludes.

The NEB Method

In the original NEB method, a path between two structures is represented as an ordered set of intermediate structures called "images." Two forces are defined on each image—a parallel force, $\boldsymbol{F}^{\parallel}$, and a perpendicular force, $\boldsymbol{F}^{\perp}$. The perpendicular force comes from the internal or intrinsic force felt by the system due to its potential energy function and is:

$$\begin{aligned} \boldsymbol{F}_i^{\text{int}} &= -\boldsymbol{g}_i \\ \boldsymbol{F}_i^{\perp} &= \boldsymbol{F}_i^{\text{int}} - \left(\boldsymbol{F}_i^{\text{int}} \cdot \hat{\boldsymbol{t}}_i\right)\hat{\boldsymbol{t}}_i, \end{aligned} \tag{1}$$

where $\boldsymbol{g}_i$ is the potential energy gradient calculated for image i and $\hat{\boldsymbol{t}}_i$ is the unit vector tangent to the path at the image (see below). The parallel force is an external force introduced to keep the different images uniformly spaced. It arises from a series of harmonic springs that are placed between adjacent images and takes the form:

$$\begin{aligned} \boldsymbol{F}_i^{\text{ext}} &= k_{i+1}(\boldsymbol{r}_{i+1} - \boldsymbol{r}_i) + k_i(\boldsymbol{r}_{i-1} - \boldsymbol{r}_i) \\ \boldsymbol{F}_i^{\parallel} &= \left(\boldsymbol{F}_i^{\text{ext}} \cdot \hat{\boldsymbol{t}}_i\right)\hat{\boldsymbol{t}}_i, \end{aligned} \tag{2}$$

where k_i is the force constant between images $i-1$ and i and $\boldsymbol{r}_i$ is the $3N$-dimensional vector of Cartesian coordinates defining the structure of image i. Finally, the total force on each image is just the sum of the two components:

$$\boldsymbol{F}_i = \boldsymbol{F}_i^{\perp} + \boldsymbol{F}_i^{\parallel}, \tag{3}$$

and the goal of the method is to make the force on each image vanish.

Since the path is defined only by the coordinates of its image structures, $\boldsymbol{r}_i$, the definition of a tangent vector at any point of the path is not trivial. In the original NEB method, the tangent at image i was defined as the vector joining images $i-1$ and $i+1$, so that:

$$\boldsymbol{t}_i = \boldsymbol{r}_{i+1} - \boldsymbol{r}_{i-1} \qquad \hat{\boldsymbol{t}}_i = \frac{\boldsymbol{t}_i}{|\boldsymbol{t}_i|}. \tag{4}$$

The projection of the forces in eqs. (1) and (2) makes it problematic to use second-order algorithms for the minimization of the forces. In the original NEB articles, a quenched molecular dynamics scheme was employed in which each image moved according to the total force acting on it. However, there was no memory of past moves because the velocities were set to zero at every step of the minimization.

Several improvements over the basic NEB method have been proposed. Among these are an alternative definition of the tangent vector, which employs the vector joining image i and either image $i-1$ or $i+1$, depending upon which one has the higher energy[10]; the "climbing image" variant for locating saddle points[11]; superlinear algorithms for minimization of the forces by using quasi-Newton methods[12,13]; and a temperature dependent implementation which takes into account the local curvature of the path.[14]

Modifications to the Method

The modifications to the original NEB algorithm proposed in this work are aimed at providing a faster convergence of the optimization procedure and at making the method more robust by eliminating the arbitrary spring forces of eq. (2).

In an earlier paper,[15] we showed that convergence of NEB calculations employing a quenched molecular dynamics scheme could be improved by moving only one of the path images at each optimization step. Here we extend this previous scheme by switching to a more efficient second-order L-BFGS[16,17] optimization method. In detail, this entails the following. At any NEB optimization step, the image i with the largest total force norm, $\|\boldsymbol{F}_i\|$, is identified, and a series of "mini-steps" is applied to it to reduce the force. These mini-steps are calculated with the L-BFGS method, which requires only the gradients and builds up an approximate Hessian during the optimization. The number of mini-steps is variable and they terminate when the force norm is reduced sufficiently (typically 0.1 times the initial $\|\boldsymbol{F}_i\|$) or when the maximum predefined number of mini-steps is reached (typically 20). This process is repeated in the next NEB step by reidentifying the image with the largest force norm and then applying the mini-step procedure. The "memory" of the L-BFGS algorithm is normally cleared between its optimizations because the approximate Hessians that it builds are not transferable between images. It should be noted that these optimizations are always minimizations of the total force $\boldsymbol{F}_i$ [eq. (3)], so that even in regions with negative curvature, such as close to saddle points, the optimizations should lead to points where the second derivative matrices are positive definite. The BFGS update method, which ensures positive definiteness, is thereby apt for this task.

Our second modification eliminates the spring forces by representing the path with a parametric interpolating spline. This is similar to the "string method" proposed by E et al.[5,18]

Consider a set of $n+1$ images, numbered successively from 0 to n, and represented by their $3N$-dimensional coordinate vectors, $\boldsymbol{r}_i$. A $3N$-dimensional interpolating spline $\boldsymbol{\varphi}(t)$ (a cubic spline in our case) can be generated from these images such that t is a continuous variable, whose value ranges from 0 to n, and such that $\boldsymbol{\varphi}(i) = \boldsymbol{r}_i$ for images i. The distance between adjacent images i and $i+1$ is calculated as the arc length along the spline and is expressed by the integral:

$$d(i) = \int_i^{i+1} \left| \frac{\mathrm{d}\boldsymbol{\varphi}(t)}{\mathrm{d}t} \right| \mathrm{d}t. \tag{5}$$

The total length of the path is $D = \sum d(i)$. If the images are to be equally spaced, they have to be placed at different points t_i along the path, such that $s(t_i)$, the length of the path from the starting point up to t_i, is:

$$s(t_i) = \int_0^{t_i} \left| \frac{\mathrm{d}\boldsymbol{\varphi}(t)}{\mathrm{d}t} \right| \mathrm{d}t = \frac{Di}{n}, \tag{6}$$

It is straightforward to solve this equation numerically and obtain the t_i values. This gives, in turn, a new set of coordinates for the images in the original path, $\boldsymbol{r}'_i = \boldsymbol{\varphi}(t_i)$, which are now evenly spaced. As shown by Wang et al.,[19] a new interpolating spline $\boldsymbol{\varphi}'(t)$ can be obtained from these points, which has the property that it follows closely the initial spline and it is approximately parametrized by arc length, which means that the length of the spline up to the point defined by t, $s'(t)$, is proportional to t itself. Since the images are defined by a regular succession of values of t ($\{0, 1, \ldots, n\}$), the corresponding values of $s'(t)$ will be regular as well, and the images will be evenly spaced in the new path $\boldsymbol{\varphi}'(t)$.

The repositioning of the images and reparametrization of the spline could be performed at every step of the NEB optimization, thereby ensuring that the images are always evenly spaced. However, we found that it is sufficient (and computationally more efficient) to apply the procedure only when the spacing of the images becomes significantly distorted.

The tangent vector for any point of the path can be also be determined from the interpolating spline. In principle, it is possible to use this tangent vector for the projection of eq. (1) as in the "string method" of E et al.[5] In our tests, though, we found that the use of this tangent led to instabilities in the optimization whereas the improved tangent proposed by Henkelman and Jónsson[10] provided much more robust behavior.

Overall, the scheme of our modified NEB method is as follows

1. From the structures of reactants, $\boldsymbol{r}_0$, and products, $\boldsymbol{r}_n$, an initial path is defined as a set of $n-1$ intermediate structures, $\boldsymbol{r}_i$. This is often done by straightforward linear interpolation between the end-point structures.
2. An interpolating spline $\boldsymbol{\varphi}(t)$ is calculated such that $\boldsymbol{\varphi}(i) = \boldsymbol{r}_i$. We employ a piecewise cubic spline for $\boldsymbol{\varphi}(i)$ with the conditions of continuity and differentiability at the image points ($t = i$) and vanishing curvature at the endpoints ($t = 0, n$).
3. The gradient, tangent vector and perpendicular force, $\boldsymbol{F}_i^{\perp}$, are obtained for each intermediate image.
4. The image with the largest force is identified and its structure is altered in order to minimize this force. The L-BFGS algorithm is used for this and is applied until the force norm is reduced below a certain threshold, relative to the initial value, or until a given number of iterations is reached.
5. A new interpolating spline is obtained with the new structure of the previous step and the lengths of the spline sections between each pair of images i and $i+1$ are calculated. To decide whether the images need to be redistributed, we monitor the ratio of the largest to the smallest inter-image distances along the path. If this is above a certain threshold (typically 1.5), the images are redistributed and a new spline is calculated that will be approximately arc-length parametrized.
6. The gradient, tangent and force are recalculated for the images that have moved or whose tangent definition has changed.
7. Step 4 is repeated until the convergence criteria for the optimization are satisfied. Typically this requires that the value of the largest RMS force for an image falls below a specified threshold value.

As an aside, we note that each image structure is represented by a $3N$-dimensional vector of Cartesian coordinates. In many cases of interest, though (including all of those presented in the next section), this set is redundant as it includes degrees of freedom for the global rotational and translational motions for the system. These are straightforward to eliminate using standard techniques (see, for example, chapter 8 of ref. 20) with minimal changes to the above scheme.

Tests and Results

The above modifications to NEB were implemented in the DYNAMO program[20] which is a Fortran 90/95 library designed for performing simulations of biomolecular systems with hybrid QM/MM potentials. With this program we tested the performance of the NEB implementation described in our previous work[15] and the same method with the improvements proposed here. For convenience we term these methods o-NEB (original NEB) and s-NEB (spline NEB), respectively.

Tests were performed on the following systems:

Cyclohexane

The interconversion between the chair and twist-boat conformations of cyclohexane was studied with a simple MM model (the OPLS-AA[21] force field).

Blocked Alanine

The interconversion between the different conformations of blocked alanine (bALA) was studied with the OPLS-AA force field. We considered the α, C_5, C_7^{ax} and C_7^{eq} conformations and the 6 possible transition paths between them. bALA, also known as the alanine dipeptide, has been extensively studied,[22,23] since it is a simple system but with enough complexity to show several minima and reaction paths.

1,2-Difluoroethane

The complete 360° rotation about the C—C bond in 1,2-difluoroethane was studied with the AM1 semiempirical QM method.[24] The initial path was built taking the *anti* and two *gauche* rotamers as intermediates.

Triazene

The 1,3 proton shift in triazene (N_3H_3) has been studied in solution with QM/MM methods.[25] Here we studied the bimolecular reaction with an intervening water molecule in vacuum using the AM1 QM Hamiltonian.

Triptycyl[4]helicene

This and similar compounds have been studied by Kelly et al.[26] as prototypes of molecular motors. The rotation about the triptycene–[4]helicene bond was again studied using the AM1 method.

It should be noted that the aim of these tests was to compare the efficiencies of the s-NEB and o-NEB algorithms and not to determine quantitative results for reaction paths or activation energies. If this were the case, the calculations would have to be repeated with higher-level QM potentials.

Table 1. Number of Gradient Evaluations Needed to Obtain Converged Paths for the Test Systems.

	Gradient evaluations		
System	o-NEB	s-NEB	Reduction (%)
Cyclohexane	3,672	1,638	55.4
bALA ($C_7^{eq} \rightarrow C_5$)	44,156	6,035	86.3
bALA ($C_7^{eq} \rightarrow C_7^{ax}$)	108,972	10,906	90.0
bALA ($C_7^{eq} \rightarrow \alpha$)	83,585	9,783	88.3
bALA ($C_5 \rightarrow C_7^{ax}$)	114,294	12,599	89.0
bALA ($C_5 \rightarrow \alpha$)	46,420	6,924	85.1
bALA ($C_7^{ax} \rightarrow \alpha$)	32,599	5,795	82.2
1,2-Difluoroethane	2,276	1,178	48.2
Triazene	7,295	2,852	60.9
Triptycyl[4]helicene	149,625	11,108	92.6

o-NEB: the NEB method from ref. 15; s-NEB: the modified algorithm proposed in this work.

The initial paths for all the test cases were created with 21 images by linearly interpolating 19 structures between the initial and final states. The exception was the path for the rotation barrier in 1,2-difluoroethane, which was created by joining three sub-paths linearly interpolated between the three different rotamers (31 images in total). The NEB calculations were run until the value of the RMS force on every image fell below 0.02 kJ mol^{-1} Å^{-1}. For the o-NEB calculations a spring force constant of $k_i = 500$ kJ mol^{-1} Å^{-2} was used.

Table 1 shows the number of gradient evaluations needed in each case to reach convergence. In all the systems the final paths obtained with both o-NEB and s-NEB are virtually identical, which shows that the modifications proposed here do not change the behavior of the method in this respect. It can be observed that the number of gradient evaluations for every system is significantly reduced, by around 50% for the smaller systems but in excess of 90% for the larger and more complicated cases. As gradient evaluation is the most expensive part of the calculation and the time required to manipulate the splines is comparatively small, this means that the s-NEB calculations are up to ten times faster than those with the o-NEB method.

As examples, we show in Figure 1 the energy profiles obtained for the transitions calculated for the bALA system. The NEB method produces smooth paths for all cases. It can be seen, for instance, that the transformation $C_7^{eq} \rightarrow C_5 \rightarrow \alpha$ (blue in the figure) has an almost minimal activation energy (the highest transition state energy is hardly above that of the α conformation). However, when the direct $C_7^{eq} \rightarrow \alpha$ path (red in the figure) is calculated, a higher activation energy is found. When examined, the paths are found to be clearly distinct, as, for example, the rotation about the C_α—C bond is made in different directions. For the direct transformation, there is a rotation of −135.5° of the $C_\beta C_\alpha CO$ dihedral, whereas the transformation through C_5 has a rotation of 224.5° (87° up to the C_5 conformation).

This serves to illustrate a feature common to NEB and most other path optimization methods: they can only provide "local" optimum paths, the results being dependent on the initial guess when starting the optimization. In this case, the initial guesses were linear interpolations between the initial and final structures, which are obviously not the same for the transformations just discussed, and this leads to different paths across different regions of the potential energy surface. Thus, optimized paths should be sought from as many pairs of different initial and final structures as possible.

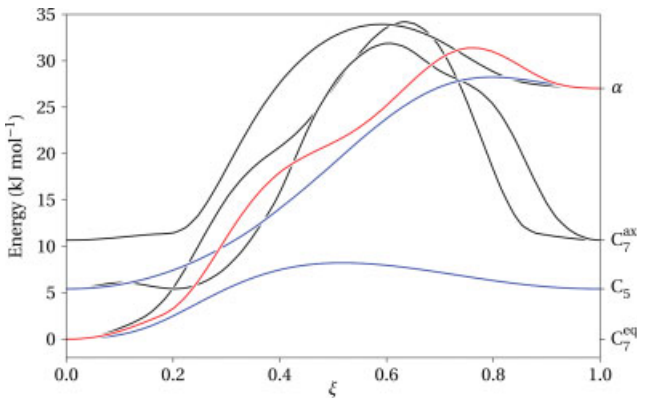

Figure 1. Energy profiles for the conversions between the four different conformers of blocked alanine obtained with the s-NEB procedure. ξ is the normalized path length: $\xi = 0$, reactants; $\xi = 1$, products. The energies of the four conformers are marked on the right. In color, the paths mentioned in the text.

A further example is shown in Figure 2, where the obtained energy profile for the triptycyl[4]helicene rotation is displayed. Kelly et al.[26] have reported a discontinuous energy profile when considering a distinguished reaction coordinate for the rotation. With the present method, however, no reaction coordinate is defined *a priori* and a continuous profile is obtained. This energy profile is basically the same as that presented in ref. 14, showing that the modifications proposed in this work do not change the results given by NEB, but rather its efficiency.

We also tested the quality of the saddle point structures that could be obtained from the spline interpolation. To do this, we generated a cubic interpolation of the energy profile[10] for each path and estimated the position of the saddle point as the point t_s with

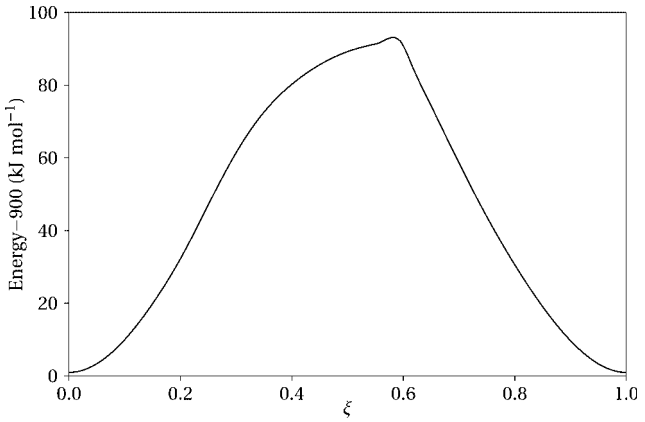

Figure 2. Energy profile for a 120° rotation around the central C–C bond in triptycyl[4]helicene obtained with the s-NEB procedure. ξ is the normalized path length: $\xi = 0$, reactant; $\xi = 1$, product.

Table 2. Quality of Two Different Estimations for the Saddle Point.

	Closest image		Interpolated	
System	$\|\Delta E\|$	RMS	$\|\Delta E\|$	RMS
Cyclohexane	0.0984	0.03105	0.0004	0.02448
bALA ($C_7^{eq} \rightarrow C_5$)	0.0167	0.03287	0.0023	0.01454
bALA ($C_7^{eq} \rightarrow C_7^{ax}$)	0.0906	0.03570	0.0027	0.01681
bALA ($C_7^{eq} \rightarrow \alpha$)	0.1382	0.05228	0.0046	0.01794
bALA ($C_5 \rightarrow C_7^{ax}$)	0.0003	0.01107	0.0015	0.00939
bALA ($C_5 \rightarrow \alpha$)	0.0121	0.02873	0.0031	0.01694
bALA ($C_7^{ax} \rightarrow \alpha$)	0.0227	0.02311	0.0014	0.00831
1,2-Difluoroethane	0.0823	0.04012	0.0000	0.00029
Triazene	0.2575	0.00841	0.0226	0.00343
Triptycyl[4]helicene	0.7725	0.19167	6.5291	0.13729

The energy difference, $|\Delta E|$, and the RMS coordinate deviation in the structure with respect to the optimized saddle point are given for the image with the highest energy in the path and for the approximate saddle point obtained by interpolation. Energy difference is measured and in kJ mol^{-1}. RMS deviation in angstrom.

the highest energy along the path. If an energy profile had several maxima, we selected the highest one only. Using the predicted positions of the saddle point, approximate saddle point structures were obtained from the path splines as $\boldsymbol{\varphi}(t_s)$. These structures were then compared with those of the "true" saddle points found for each path using standard second-derivative-based methods. Table 2 shows the absolute energy differences and the RMS coordinate differences between the estimated (interpolated) saddle point structures and the optimized ones. In the absence of interpolation, the best estimate for the saddle point would be the image with the highest energy in the path. The comparison between this highest energy image and the optimized saddle point is also shown in Table 2. Both the closest image and interpolated structures are good approximations but the latter have consistently smaller RMS coordinate differences and, in all but two cases, smaller absolute energy differences.

Conclusions

The modifications to the NEB algorithm proposed here have been tested on chemical systems of different complexities. The results show a clear improvement in performance compared with a more traditional NEB method as the number of gradient evaluations (and, hence, computation time) can be reduced by 90% or more for complicated systems.

The increased efficiency is mostly due to the use of a second order optimization algorithm. This was evident during the early stages of our work when the spline description of the path had yet to be implemented. Rationalization is straightforward, as the L-BFGS minimization works on all but one of the degrees of freedom of the system, whereas the parametric representation of the path and image repositioning affect only a single degree of freedom. This observation can be related to a result in ref. 15, which found that an analytical minimization of the spring forces did not yield significant efficiency enhancements.

In addition to the performance improvement, the use of a parametric spline description of the path has other advantages. First, the arbitrary spring forces of the original NEB are not needed, so there is one less parameter to be specified. Second, interpolated structures along the path are readily obtained, either for estimating saddle point structures or for increasing the resolution of the path sampling. Third, it would be relatively easy to implement an adaptive variant of the method in which the number of images along the path changes dynamically as its length varies.

Acknowledgements

The authors thank the Institut de Biologie Structurale—Jean-Pierre Ebel, the Commissariat à l'Energie Atomique and the Centre National de la Recherche Scientifique.

References

1. McKee, M. L.; Page, M. In Reviews in Computational Chemistry; vol. IV; Lipkowitz, K. B.; Boyd, D. B., Eds.; VCH: New York, 1993; ch. 2, pp. 35–65.
2. Cerjan, C. J.; Miller, W. H. J Chem Phys 1981, 75, 2800.
3. Baker, J. J Comput Chem 1986, 7, 385.
4. González, C.; Schlegel, H. B. J Phys Chem 1990, 94, 5523.
5. E, W.; Ren, W.; Vanden-Eijnden, E. Phys Rev B 2002, 66, 052301.
6. Elber, R.; Karplus, M. Chem Phys Lett 1987, 139, 375.
7. Choi, C.; Elber, R. J Chem Phys 1991, 94, 751.
8. Crehuet, R.; Bofill, J. M. J Chem Phys 2005, 122, 234105.
9. Jónsson, H.; Mills, G.; Jacobsen, K. W. In Classical and Quantum Dynamics in Condensed Phase Simulations; Berne, B. J.; Ciccotti, G.; Coker, D. F., Eds.; World Scientific: Singapore, 1998; ch. 16, pp. 385–404.
10. Henkelman, G.; Jónsson, H. J Chem Phys 2000, 113, 9978.
11. Henkelman, G.; Uberuaga, B. P.; Jónsson, H. J Chem Phys 2000, 113, 9901.
12. Chu, J.-W.; Trout, B. L.; Brooks, B. R. J Chem Phys 2003, 119, 12708.
13. Trygubenko, S. A.; Wales, D. J. J Chem Phys 2004, 120, 2082.
14. Crehuet, R.; Field, M. J. J Chem Phys 2003, 118, 9563.
15. Crehuet, R.; Thomas, A.; Field, M. J. J Mol Graph Model 2005, 24, 102.
16. Liu, D. C.; Nocedal, J. Math Program B 1989, 45, 503.
17. Nocedal, J. Math Comp 1980, 35, 773.
18. E. W.; Ren, W.; Vanden-Eijnden, E. J Phys Chem B 2005, 109, 6688.
19. Wang, H.; Kearney, J.; Atkinson, K. In Curve and Surface Design: Saint-Malo 2002; Lyche, T.; Mazure, M.-L.; Schumaker, L. L., Eds.; Nashboro Press: Brentwood, TN, 2003; pp. 387–396.
20. Field, M. J. A Practical Introduction to the Simulation of Molecular Systems; Cambridge University Press: Cambridge, 1999.
21. Jorgensen, W. L.; Maxwell, D. S.; Tirado-Rives, J. J Am Chem Soc 1996, 118, 11225.
22. Apostolakis, J.; Ferrara, P.; Caflisch, A. J Chem Phys 1999, 110, 2099.
23. Bolhuis, P. G.; Dellago, C.; Chandler, D. Proc Natl Acad Sci USA 2000, 97, 5877.
24. Dewar, M. J. S.; Zoebisch, E. G.; Healy, E. F.; Stewart, J. J. P. J Am Chem Soc 1985, 107, 3902.
25. Fdez. Galván, I.; Aguilar, M. A.; Ruiz-López, M. F. J Phys Chem B 2005, 109, 23024.
26. Kelly, T. R.; Sestelo, J. P. In Molecular Machines and Motors; No. 99 in Structure & Bonding; Sauvage, J.-P., Ed.; Springer: Berlin, New York, 2001; ch. 2, pp. 19–53.